SLAC–PUB–4966
April 1989
(E/I)

TRIGGERING AND DATA ACQUISITION ASPECTS OF SSC TRACKING*

GAIL G. HANSON, BOGDAN B. NICZYPORUK† AND ANDREA P. T. PALOUNEK‡
Stanford Linear Accelerator Center, Stanford University,
Stanford, California 94309, USA

ABSTRACT

Possible conceptual designs for wire chamber tracking systems which meet the requirements for radiation damage and rates in the SSC environment are discussed. Computer simulation studies of tracking in such systems are presented. Results of some preliminary pattern recognition studies are given. Implications for data acquisition and triggering are examined.

1. INTRODUCTION

The primary motivation for the SSC is the expectation that it will lead to new discoveries, such as Higgs bosons, supersymmetric particles, heavy W's or Z's, new heavy fermions, or composite particles with masses in the TeV region. Such particles would be produced in the central rapidity region, that is, over $\pm$ 3 units of rapidity, and would decay to high-p_T electrons, muons, or jets, often with large missing transverse energy (E_T) due to undetectable neutrinos. In order to fully investigate the physics opportunities in this regime, a general-purpose detector which includes charged particle tracking is needed. Some of the most important functions of charged particle tracking include:

1. Identification of electrons.
2. Separation of multiple interactions within the same bunch crossing.
3. Matching electrons, muons, and jets to the correct vertex.
4. Electron charge sign determination.
5. Improving e/π separation.
6. Identification of secondary vertices.
7. Identification of τ leptons.

* Work supported by the Department of Energy, contract DE–AC03–76SF00515.

† Permanent Address: CEBAF, Newport News, Virginia 23606.

‡ Present Address: Lawrence Berkeley Laboratory, Berkeley, California 94720.

Presented at the Workshop on Triggering and Data Acquisition for Experiments at the Supercollider, Toronto, Canada, January 16–19, 1989

8. Invariant mass or momentum cuts.
9. Improving the missing E_T measurement and verifying calorimeter data.
10. Establishing the credibility of new physics and providing redundancy.

Many of these functions require momentum measurement in a magnetic field.

Tracking at the SSC at the full design luminosity of 10^{33} cm^{-2}s^{-1} is expected to be a difficult problem. The limitations imposed by rates and radiation damage are severe. However, the dominant constraint is the combination of occupancy and double-hit resolution. Single events from new physics at the SSC have many (several hundred) charged particle tracks and are further complicated by curling tracks in a magnetic field, photon conversions, hits from events from out-of-time bunch crossings, and multiple interactions within the same bunch crossing. These problems can probably be solved, but at the cost of mechanical complexity and many signal channels.[1] We report here on a computer simulation study of tracking in complex SSC events and discuss some implications for triggering and data acquisition.

2. TRACKING SYSTEM REQUIREMENTS

2.1 The SSC Environment

The design luminosity, $\mathcal{L}$, of the SSC is 10^{33} cm^{-2}s^{-1} with an energy of 40 TeV in the center of mass. The inelastic cross section, σ, at 40 TeV is expected to be about 100 mb, which gives 10^8 interactions per second at the design luminosity. The bunch separation is 4.8 m, so the time between bunch crossings, t_B, is 16 ns, which leads to an average number of interactions per bunch crossing, n_I, of 1.6 at the design luminosity. Most of these interactions are minimum bias events or low-p_T hard scattering processes in which particle production is expected to be uniform in rapidity. The average charged particle multiplicity per unit of rapidity, n_c, is expected to be 7.5 over the rapidity range $|\eta| < 6$.[2] Figure 1 (from Ref. 2) shows the resulting charged particle flux and annual dose as a function of perpendicular distance from the beam for standard SSC operating conditions.

2.2. Rates and Radiation Damage

Radiation damage and rate limitations impose severe constraints on charged particle tracking detectors at the SSC, as described in several references.[1,3] These constraints are summarized here since they are necessary considerations for the design of any SSC tracking system.

A tracking system for the SSC is assumed to be made up of wires or other detectors running (nearly) parallel to the beam line. The width, w, of a cell is

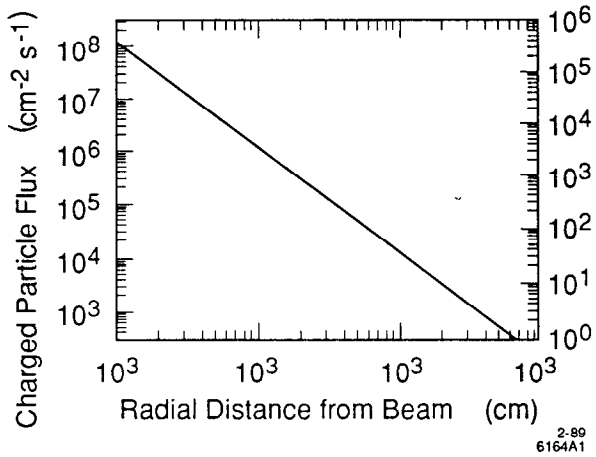

Fig. 1. The charged particle flux and annual dose as a function of perpendicular distance from the beam under standard SSC operating conditions (from Ref. 2).

assumed to be equal to the height, h, and the drift distance, d, is half the cell width. The ionization rate, α, in the gas is assumed to be 100 electrons/cm. The gas gain, G, is assumed to be 2×10^4, which is rather low.

The flux of particles per unit length (ℓ) of wire in a cell at radius r is given by

$$\frac{d^2n}{d\ell\, dt} = \frac{n_c\, w\, \sigma\, \mathcal{L} \sin\theta}{2\,\pi\, r^2}, \tag{1}$$

where θ is the angle relative to the beam direction. The ionization produced by a charged particle at angle θ is $h\alpha/\sin\theta$, so the ionization per unit length of wire is independent of θ. Thus the current draw per wire, I, for a layer of wires of length L at radius r is given by

$$I = \frac{n_c\, w\, h\, \sigma\, \mathcal{L}\, G\, e\, \alpha\, L}{2\,\pi\, r^2}, \tag{2}$$

where e is the electron charge. A layer of 4 mm wide cells at a radius of 50 cm covering $|\eta| < 1.5$ ($L = 213$ cm) will draw 0.52 μA/wire. The limit of acceptable current draw before breakdown will occur is about 1 μA/wire.

Wire chamber lifetimes are measured in deposited charge per unit length of wire before a decrease in gain occurs due to the buildup of material on the wires. For the above example, the collected charge over a chamber lifetime of five years (5×10^7 s) would be 0.12 C/cm. Chamber lifetimes of 1.0 C/cm have been measured under

very clean laboratory conditions.[4] For the purposes of a realistic experiment, it is probably best to assume a chamber lifetime about an order of magnitude below this.

Changes in gain for wire chambers have been observed at the level of 10^5 particles/cm-s at a gas gain of $\sim 4 \times 10^5$ due to space charge buildup.[5] The particle flux is given by Eq. 1. For the above example, the flux would be 1.9×10^4 particles/cm-s at $\theta = 90°$ where the flux is maximum. Since the gas gain must be much smaller than 4×10^5 because of current draw and lifetime considerations, space charge should not be an important limitation.

The hit rate per wire, R, for SSC tracking chambers is quite large and is given by

$$R = \frac{n_c \, \eta_{max} \, \sigma \, \mathcal{L} \, w}{\pi \, r} \tag{3}$$

for chambers covering $|\eta| < \eta_{max}$. For the above example, the hit rate per wire would be 2.9 Mhz. Existing electronics can probably handle rates of $\sim$ 10 Mhz.

A very serious limitation for tracking systems at the SSC is occupancy. Since the time between bunch crossings at the SSC is shorter than the resolving time of a typical drift chamber cell, the cell is sensitive to several bunch crossings. The occupancy, O, is given by

$$O = \frac{2 \, n_c \, \eta_{max} \, n_I \, n_B \, d}{\pi \, r}, \tag{4}$$

where n_B is the number of bunch crossings during the resolving time of the cell. n_B is given by

$$n_B = 1 + \mathrm{int}\,(t_R/t_B)\left[\, 2 - t_B/t_R - (t_B/t_R)\,\mathrm{int}\,(t_R/t_B) \,\right], \tag{5}$$

where t_R is the resolving time of the cell, d/v_D, for drift velocity v_D, and $\mathrm{int}\,(x)$ is the largest integer $\leq x$. Actually, n_B is very close to $t_R/t_B = d/(v_D \, t_B)$. A 4 mm wide cell (2 mm drift) has a resolving time of 40 ns for a typical drift velocity of 50 μm/ns and is therefore sensitive to 2.6 bunch crossings. A layer of such cells at a radius of 50 cm and covering a rapidity range $|\eta| < 1.5$ would have an occupancy of 12% per cell. It is guessed that an occupancy of $\sim$ 10% is reasonable, but a realistic answer depends on the effects on pattern recognition and track finding, which are discussed in more detail in Section 3. The real limitation to occupancy is due to the double-hit resolution because of the loss of information. A faster gas,[6] such as mixtures of CF_4 with a saturated drift velocity of 125 μm/ns, would improve the situation considerably by reducing the occupancy for a given cell width. Silicon

microstrip or pixel devices have very small "cells" and so avoid the problem of high occupancy, but they must either be able to operate in the higher radiation environment at small radius or be built into a very large silicon tracking system.

The rates given above are based only on particles produced in an interaction and must be increased by a factor of 2–4 because of curling tracks in a magnetic field, converted photons, and albedo particles leaking out of the front face of the calorimeter. Regardless of pattern recognition considerations, the effects on current draw and chamber lifetime must be carefully considered in the design of any SSC tracking system based on wire chambers.

2.3. Tracking System Considerations

2.3.1. Cell Size and Shape. For the reasons discussed in the previous Section, cell widths are constrained to a few mm. Straw tube chambers are a natural candidate for a small cell design. Construction possibilities for a tracking system made of straw tubes are discussed in Refs. 1 and 7. A tracking system based on jet cells, such as shown in Fig. 2, might also be considered. However, since the jet cell would be only a few mm wide and would be tilted so that the electron drift trajectories in a large magnetic field would be perpendicular to the sense wire planes, the advantages of a jet cell, e.g., uniform drift electric field over most of the cell and long track segments in one cell, are lost. In addition, there would be large forces on the endplates due to the tension of the large number of field wires. Also, as in any open wire geometry, it would be difficult to devise a mechanism to support the long sense wires in order to maintain electrostatic stability. On the other hand, straw tubes provide the possibility of supports for the wires.

The straws are typically made of aluminized polyester film (Mylar) or polycarbonate (Lexan) with wall thicknesses of about 30 μm. Several layers of straw tubes can be glued together to form superlayers which would be rigid, mechanically stable structures. Within each superlayer the layers can be staggered by half the cell width in order to allow hits from out-of-time bunch crossings to be rejected and resolve left-right ambiguities, as illustrated in Fig. 3. By dividing the chamber into superlayers, locally identifiable track segments can be obtained at the pattern recognition stage. The track segments can then be linked to form tracks. There must be a sufficient number of layers in the superlayers to provide redundancy.

2.3.2. z-Reconstruction. The wires or other sensing elements are assumed to run parallel, or nearly parallel, to the beam direction, or z-axis. The three conventional methods for measuring the coordinate along a wire are charge division, small-angle stereo, and cathode strips (or pads) running perpendicular to the wires. A fourth, less conventional, method is the time-difference method which probably has similar resolution to charge division, but may be worth further consideration.

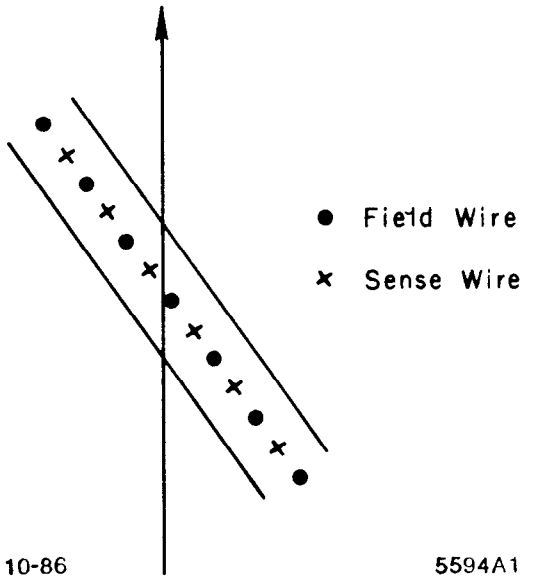

Fig. 2. Narrow tilted jet cell with radial track.

Charge division, at best (high gas gain $\sim 10^5$), gives z-coordinate resolution of about 1% of the length of the wire. Since the wires in an SSC tracking system would be quite long (3–6 m) in order to cover the required rapidity range, the resolution would be only 3–6 cm. Since low gas gain is needed to reduce current draw and increase chamber lifetime, the resolution in an SSC tracking system would be even worse. Also, charge division requires electronics readout at both ends of the wire which increases the complexity of a system with a large number of wires. For these reasons charge division does not appear to be a practical method for measuring the z-coordinate in an SSC tracking system.

Small-angle stereo ($\sim 3°$) wires typically give z-coordinate resolution of a few mm (the drift distance resolution divided by the stereo angle). The same electronics for time measurement can be used for all wires. In a system of superlayers of straw tubes, every other superlayer might be small-angle stereo. However, in complex SSC events it may be difficult to associate the hits on stereo wires with the correct tracks.

Azimuthal cathode strips or pads can give a z resolution of better than 1 mm. They might be included on the outer surfaces of the superlayers to aid in bunch assignment and reducing stereo ambiguities. However, they present added electrical and mechanical difficulties, as well as increasing the number of readout channels.

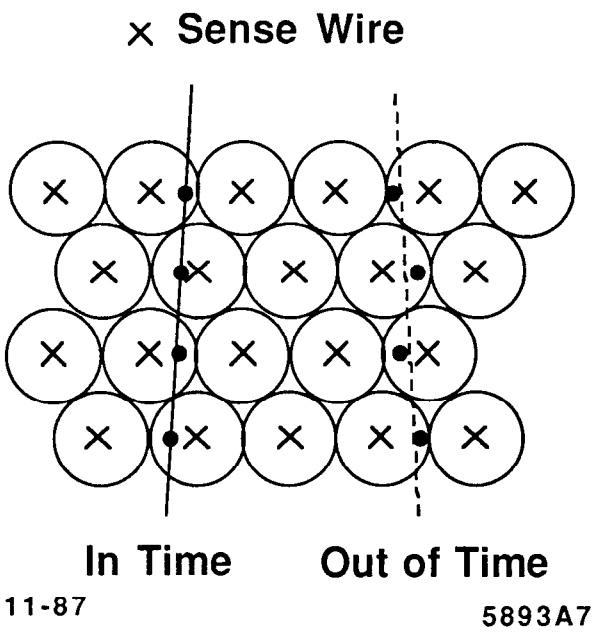

Fig. 3. Layers of straw tubes in a superlayer with every other layer staggered by the straw tube radius. A single in-time track will appear as a series of hits on the wires on alternate sides of the track. The left-right ambiguity is easily resolved locally. A track from an out-of-time bunch crossing will produce hits which are displaced from possible tracks by at least 16 ns in drift time.

2.3.3. Momentum Measurement. At the 1987 Berkeley Workshop[8] an examination of the requirements for momentum resolution based on the physics led to the criterion that the sign of the charge for electrons should be measured for $p_T \leq 0.5$–1.0 TeV/c. The momentum resolution is given by[9]

$$\frac{\sigma_{p_T}}{{p_T}^2} = \sqrt{\frac{720}{1+5/N}} \left(\frac{\sigma_x}{0.3\, q\, B\, D^2 \sqrt{N}} \right) \quad , \tag{6}$$

where p_T is the transverse momentum of the particle in GeV/c, q is the charge in units of the electron charge, σ_x is the spatial resolution in m, B is the magnetic field in Tesla, D is the track length in m, and N is the number of measurements, assumed to be equally spaced. Momentum resolution of $\sim 30\%$ is needed for charge sign determination. As an example, charge sign determination for $p_T \lesssim 450$ GeV/c could be obtained with a spatial resolution of 150 μm, 2 Tesla magnetic field, track length of 1 m, and 100 measurements.

2.3.4. Electronics Considerations. As discussed above, wire chambers for SSC tracking are required to have a small-cell design. Straw tube chambers seem to be particularly suitable. Since these chambers must have low gas gain, preamplifiers need to have low noise. Small-cell wire chambers probably have no multihit capability within a single event since the width of the pulses is approximately equal to the maximum drift time across the cell, so careful pulse shaping and digitization are probably not useful.. A pole-zero filter to suppress the $1/t$ tail from pulses from previous bunch crossings is needed. Fast leading-edge timing using a threshold, double-threshold, or constant-fraction discriminator is dictated. The resolution for drift-time measurement should be $\lesssim$ 500 ps, which corresponds to 25–60 μm depending on the drift velocity. All of the electronics – preamplifiers, pulse shapers, discriminators, time measurement electronics, track processors to find track segments, and digital or analog pipelining – should be located on the tracking detector in order to reduce the number of cables and processing time. The implication is that the electronics must have low power dissipation as well as radiation hardness. Electronics for cathode strips or pads is also needed.

2.3.5. Example of an SSC Tracking System. A large solenoid detector based on more-or-less "conventional" technology was discussed at the 1987 Berkeley Workshop.[10] Calorimetry and tracking were located inside a large superconducting solenoid with 2 Tesla field. A schematic view of the Large Solenoid Detector is shown in Fig. 4.

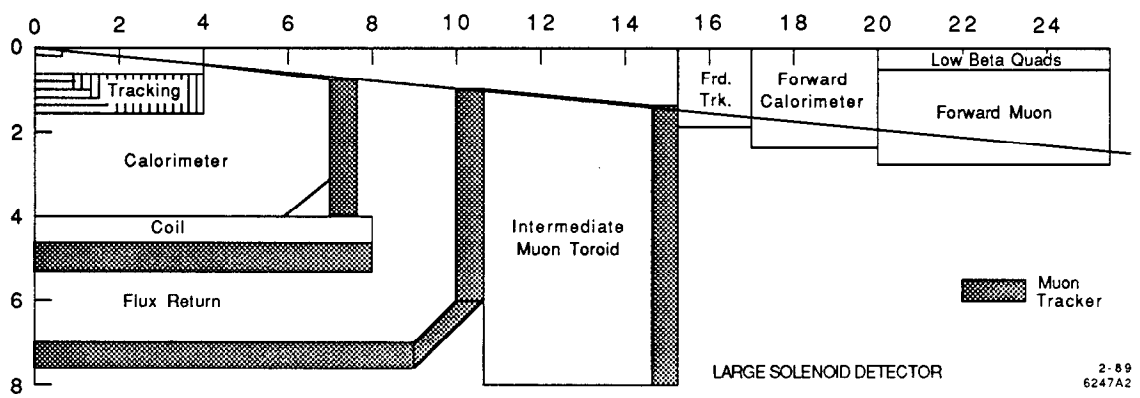

Fig. 4. Schematic view of the Large Solenoid Detector from the 1987 Berkeley Workshop.[10]

Table 1. Summary of Large Solenoid Detector Central Tracking System (from Ref. 10)

Superlayer Number	Inner Radius (cm)	Module Thickness (cm)	Half Length (cm)	Straw Diameter (mm)	Rapidity Range	Cell Occupancy (%)
1	40	2.7	85.2	3.92	1.50	12.1
2	48	2.7	85.2	3.92	1.34	9.1
3	56	2.7	119.0	3.92	1.50	8.8
4	64	2.7	119.0	3.92	1.38	7.0
5	72	4.1	119.0	5.89	1.28	13.0
6	80	4.2	170.0	6.04	1.50	14.5
7	88	4.2	170.0	6.17	1.41	12.9
8	96	4.3	170.0	6.28	1.34	11.6
9	104	4.4	170.0	6.38	1.27	10.5
10	112	4.5	238.5	6.47	1.50	11.9
11	120	4.5	238.5	6.55	1.44	10.9
12	128	4.6	238.5	6.61	1.38	10.0
13	136	4.6	238.5	6.68	1.33	9.3
14	144	4.6	238.5	6.73	1.28	8.5
15	152	4.7	238.5	6.78	1.23	7.9

The tracking detector design for the Large Solenoid Detector was divided into central tracking ($|\eta| \lesssim 1.2$) and intermediate tracking ($1.2 \lesssim |\eta| < 2.5$). The central tracking system was assumed to be built of straw tubes of radii from 2 to 3.5 mm parallel or nearly parallel to the beam direction. The straws are assumed to be at atmospheric pressure. Eight layers of straws are glued together to form superlayers. Within each superlayer the layers are staggered by half the cell width, as illustrated in Fig. 3. Every other superlayer is small-angle stereo ($\sim 3°$) in order to measure the coordinate along the wire. Azimuthal cathode pads or strips are included on the outer surfaces of the superlayers. The central tracking system extends radially from 40 cm to 160 cm with 15 superlayers in all. Only the superlayers at radii greater than 50 cm are expected to be operable at the full design luminosity. Assuming a spatial resolution of 150 μm, the momentum resolution which can be obtained with such a system is $0.54p_T$ (TeV/c) using only wires at radii larger than 50 cm. If the particles are constrained to come from the interaction region, the momentum resolution would improve to $0.26p_T$. The total number of cells is 122,368. The total number of radiation lengths is 8% for a particle traversing the central tracking chambers at 90°. The Large Solenoid Detector central tracking system geometry is summarized in Table 1.

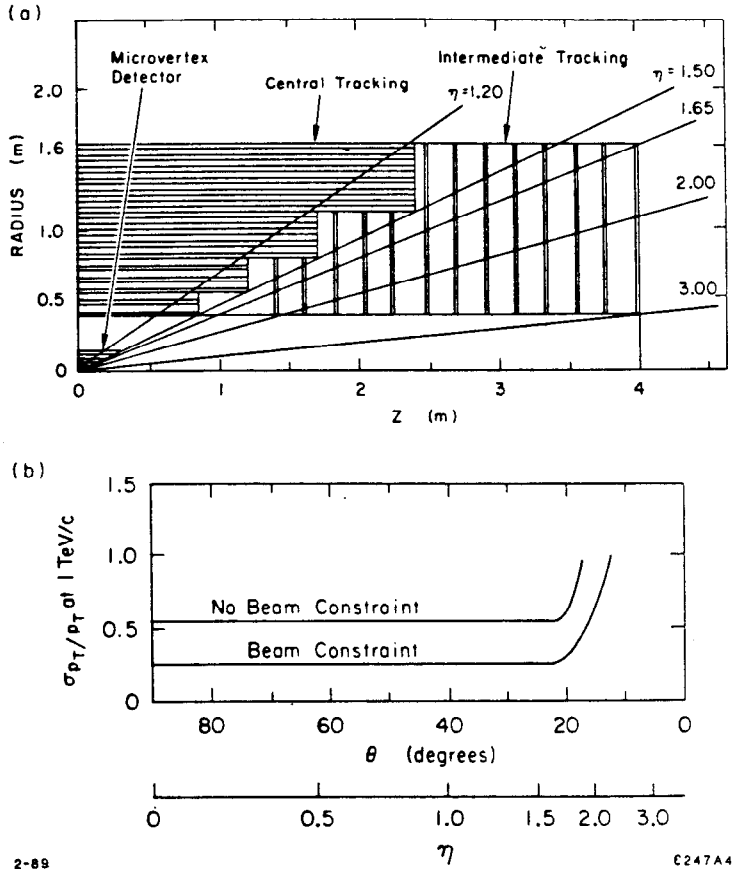

Fig. 5. (a) Schematic view of central and intermediate tracking systems in the Large Solenoid Detector. (b) Momentum resolution as a function of polar angle and rapidity in the Large Solenoid Detector for the 13 superlayers at radii > 50 cm in the central tracking system and including intermediate tracking (from Ref. 10).

In order to provide momentum measurement for $1.2 \lesssim |\eta| < 2.5$, the Large Solenoid Detector included tracking in the intermediate region to take over where the central tracking ends. Two options were considered: planes of parallel wires and radial chambers. The options for intermediate tracking have not yet been worked out in as much detail as the central tracking.

The central and intermediate tracking systems for the Large Solenoid Detector are shown in Fig. 5(a), and the momentum resolution as a function of polar angle and rapidity is shown in Fig. 5(b).

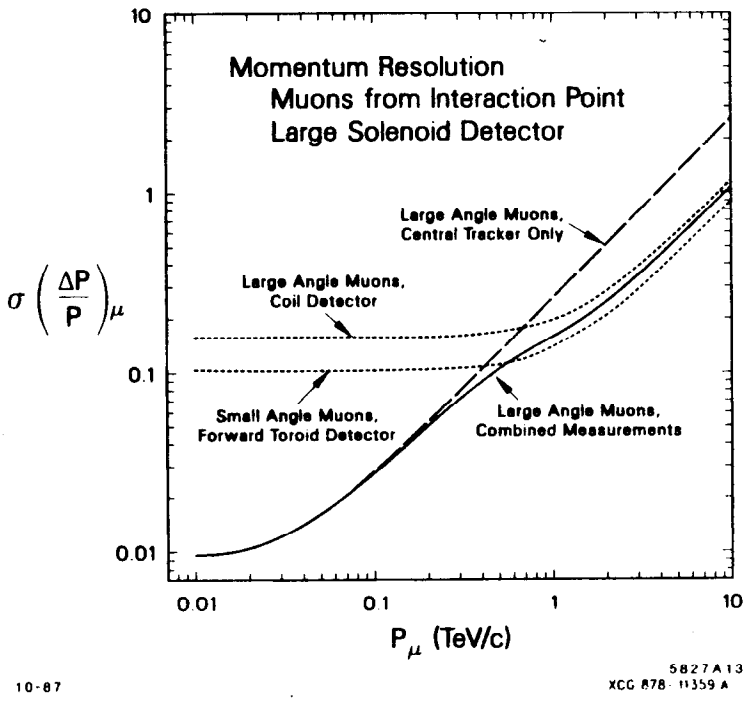

Fig. 6. Momentum resolution for measurement of large-angle and small-angle muons in the Large Solenoid Detector (from Ref. 10).

2.3.6. Muon Identification and Momentum Measurement. Another very important function of charged particle tracking in an SSC detector is muon identification and momentum measurement. The muon detection system in the Large Solenoid Detector[10] integrates muon momentum measurements with the central tracking detector, the large solenoid magnetic flux return yoke, and the calorimetry. Muons at small angles are measured by means of conventional magnetized iron toroids placed around the beam pipe. The relationship of the muon detection elements is shown in Fig. 4. In this conceptual design the spatial precision of points along the orbit in the bending direction is assumed to be 50 μm. The momentum resolution obtainable for both large-angle and small-angle muons is shown in Fig. 6. In both cases the momentum resolution is dominated by multiple Coulomb scattering below about 500 GeV/c for measurements made outside the calorimeter or magnet iron. The momentum resolution is improved considerably

for-large-angle muons, especially for momenta below about 500 GeV/c, by combining measurements made in the central tracking system with those in the muon detection system. The momentum resolution remains at about the 10% level for momenta up to about 600 GeV/c in both the large-angle and small-angle systems.

How good does the muon momentum resolution need to be? Momentum resolution requirements for detecting the heavy Higgs boson in the mode $Higgs \rightarrow Z^0 Z^0 \rightarrow 4\ell^{\pm}$ have been examined.[11] Figure 7 shows the di-lepton invariant mass for several energy or momentum resolution functions for a 400 GeV/c^2 Higgs decaying into $ZZ \rightarrow \ell^+\ell^-\ell^+\ell^-$: (a) $\sigma_E/E = 0.15/\sqrt{E}$ (E in GeV), (b) $\sigma_{p_T}/p_T = 0.54 p_T$ (p_T in TeV/c), (c) $\sigma_E/E = 10\%$, and (d) $\sigma_E/E = 20\%$. The mass resolution in Fig. 7 (a) is quite good – a cut of $\pm$ 5 GeV/c^2 on the mass around the mass of the Z (M_Z) could be used. For Figs. 7 (b) and (c) one could still use $\Delta M_Z < 10$ GeV/c^2. However, some signal would be lost with this cut for the case of 20% resolution. The effects of momentum resolution on the Z-pair mass were then examined. Figure 8 (a)–(e) shows the Z-pair mass distribution along with the background from ZZ continuum production for a 400 GeV/c^2 Higgs boson for perfect detection and for the four energy or momentum resolutions shown in Fig. 7. We see that an energy resolution of $0.15/\sqrt{E}$ gives a Higgs peak which is indistinguishable from perfect detection because of the intrinsic width of the Higgs. The cases $0.54 P_T$ and 10% energy resolution give somewhat broader but still observable peaks at the Higgs mass. However, 20% energy resolution broadens the Higgs peak so much that it is not distinguishable from background. The conclusion was that a momentum resolution of no worse than 10% was needed to find a heavy Higgs signal for a 400 GeV/c^2 Higgs.

2.3.7. Summary of Large Solenoid Detector Parameters. The design parameters of the Large Solenoid Detector are summarized in Table 2.

3. TRACKING SIMULATION

3.1. Simulation of a Central Tracking System for the SSC

The SSC central tracking system design used for this simulation was based on that for the Large Solenoid Detector[10], described in Section 2.3.5, although it is quite general and can be used for any system of cylindrically oriented sensing elements. All parameters of the detector, such as number of superlayers, number of layers in each superlayer, minimum and maximum radius and length of each superlayer, and azimuthal spacing between sense wires can be specified independently. The parameters used are as shown in Table 1, except that we included only the outer thirteen superlayers. We used a solenoidal magnetic field of 2 Tesla. The spatial resolution was taken to be 150 μm. So far, we have simulated only axial wires, that is, wires parallel to the cylinder axis.

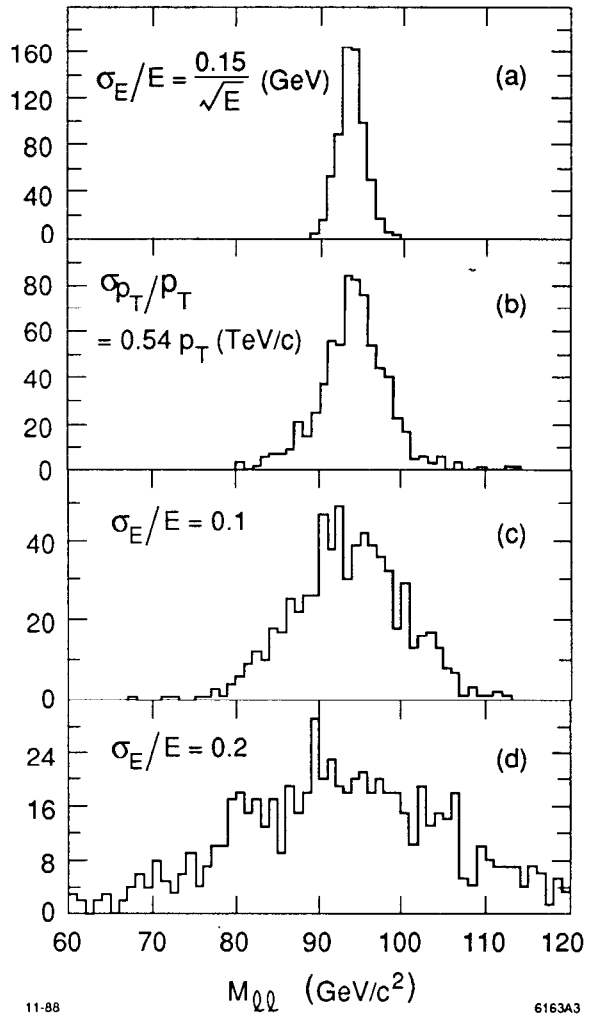

Fig. 7. Di-lepton invariant mass distributions for various energy or momentum resolutions for leptons from Higgs bosons of 400 GeV/c^2 mass decaying into $ZZ \rightarrow 4\ell^{\pm}$.

We used ISAJET[12] to generate events from interesting physics processes, such as high-p_T two-jet events or Higgs boson production, and from inelastic scattering background, for which we used minimum bias events. We used the GEANT3[13] general-purpose detector simulation package running on the SLAC IBM 3081 to simulate the interactions of the particles with the detector.

Using GEANT, the particles interact in the 8% of a radiation length of material due to straw tube walls, wires, and gas (the material was assumed to be distributed uniformly throughout the tracking volume), including photon conversion and multiple Coulomb scattering. The digitizations consist of a wire number

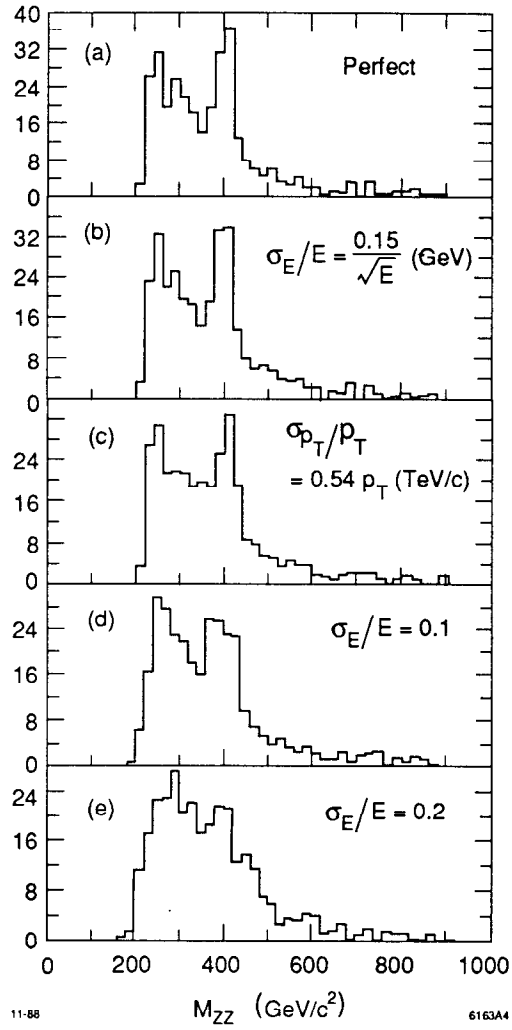

Fig. 8. Z-pair mass distributions for various energy or momentum resolutions for $H \rightarrow ZZ \rightarrow 4\ell^{\pm}$ for a 400 GeV/c^2 Higgs boson, along with the background from continuum ZZ production.

and a drift time, calculated from the distance of closest approach of a track to a wire using a drift velocity of 50 μm/ns, for each track in each layer. Background from inelastic scatterings in the same and out-of-time bunch crossings is included by superimposing the digitizations from minimum bias events. The number of bunch crossings is determined by the resolving time of the straw tube cell. At each bunch crossing the number of events to be included is determined from a Poisson distribution with a mean of 1.6 interactions per bunch crossing. Drift times from background events are then corrected for the time difference between the bunch crossing of the background event and the bunch crossing of the event of interest.

Table 2. Summary of Large Solenoid Detector Design Parameters (from Ref. 10)

SOLENOID COIL	
Inner diameter	8.2 meters
Length	16 meters
Central field	2 Tesla
Weight (including flux return)	16,450 metric tons
CENTRAL TRACKING	
Inner radius	0.40 meters
Outer radius	1.6 meters
Number of superlayers	15
Number of cells	122,368
$\|\eta\|$ coverage	< 1.2
INTERMEDIATE TRACKING (OPTIONS A & B)	
$\|\eta\|$ coverage	$1.2 < \|\eta\| < 3.0$
z position	$\|z\| < 4.0$ meters
Total number of chambers	26 (A) or 18 (B)
Total anode wires	128,000 (A) or 172,800 (B)
Total cathode pad channels	500,000 (A) or 293,760 (B)
ELECTROMAGNETIC CALORIMETER	
Depth	25 X_0
Transverse segmentation	$(\Delta\eta \times \Delta\phi)$
$\|\eta\| < 2.0$	$.02 \times .02$
$2.0 < \|\eta\| < 4.5$	$.03 \times .03$
$4.5 < \|\eta\| < 5.5$	$.03 \times .03$ to $.08 \times .08$
Longitudinal segmentation	6 X_0, 8 X_0, 11 X_0
Total number of towers	104,000
Total number of electronics channels	312,000
Weight	
Central	200 metric tons
Forward	35 metric tons
HADRONIC CALORIMETER	
Depth	10–12 λ
Transverse segmentation	$(\Delta\eta \times \Delta\phi)$
$\|\eta\| < 2.0$	$.06 \times .06$
$2.0 < \|\eta\| < 4.5$	$.06 \times .06$
$4.5 < \|\eta\| < 5.5$	$.06 \times .06$ to $.08 \times .08$
Longitudinal segmentation	2 segments
Total number of towers	19,100
Total number of electronics channels	37,200
Weight	
Central	4800 metric tons
Forward	965 metric tons
MUON SYSTEM	
Total number of electronic channels	$\sim$ 100,000
Weight of toroids	13,000 metric tons

The double-hit resolution is equal to the cell width, that is, only the earliest hit on a wire is kept. The simulation program is described in more detail in Ref. 14.

3.2. Results of the Simulation

We used the simulation described above to study tracking in SSC events. First we examined high-p_T ($p_T > 1$ TeV/c) two-jet events. Figure 9(a) shows such an event in the detector described in Section 2.3.5. Figure 9(b) shows an enlargement of the same event in the outer two superlayers in the area of the dense jet. Figure 9(c) shows the earliest hits in the cells for the tracks shown in Fig. 9(b). Hits from background events and converted photons are not shown in Fig. 9.

We can make the following observations, which still need to be quantified with high-statistics studies:

1. Although these events have very dense jets which seem at first to be impossible to resolve, when viewed on the scale of the wire spacings most of the hits appear to lie on identifiable tracks with a 2-Tesla magnetic field, particularly in the outer superlayers.
2. Eight layers in a superlayer is probably close to the optimum number because two tracks which are as close as the wire spacings produce hits only on every other layer because of the staggering. Some of these hits may be lost due to nearby curling tracks or background hits. Three tracks within the wire spacing distance would not be resolvable.
3. Although a 2-Tesla magnetic field produces curling tracks which obscure the high-p_T tracks to some extent, particularly in the inner superlayers, the effect in the outer superlayers is to spread out the tracks and, of course, remove the low-p_T tracks from consideration.

We next turned our attention to events from Higgs boson production, $pp \rightarrow HX$, with the Higgs decaying to Z^0Z^0 and both Z^0's decaying to e^+e^- or $\mu^+\mu^-$. We used a Higgs mass of 400 GeV/c^2. Such events allowed us to focus on the measurement of the high-p_T particles from the Higgs decay. Leptons from heavy Higgs decay typically have $p_T > 20$ GeV/c. Any large solid angle SSC detector must be able to measure such events. Also, these events are not as trivial to deal with as might have been naïvely guessed. There are many tracks from the underlying event and from the particles recoiling against the Higgs boson, even before adding the hits from background interactions. For these events we used the full simulation as described in the previous Section. An example of a Higgs event in the simulated central tracking system is shown in Fig. 10. We generated ~ 200 such events.

The fully-simulated events, including adding digitizations from minimum bias background events and removing digitizations within the double-hit resolution, had

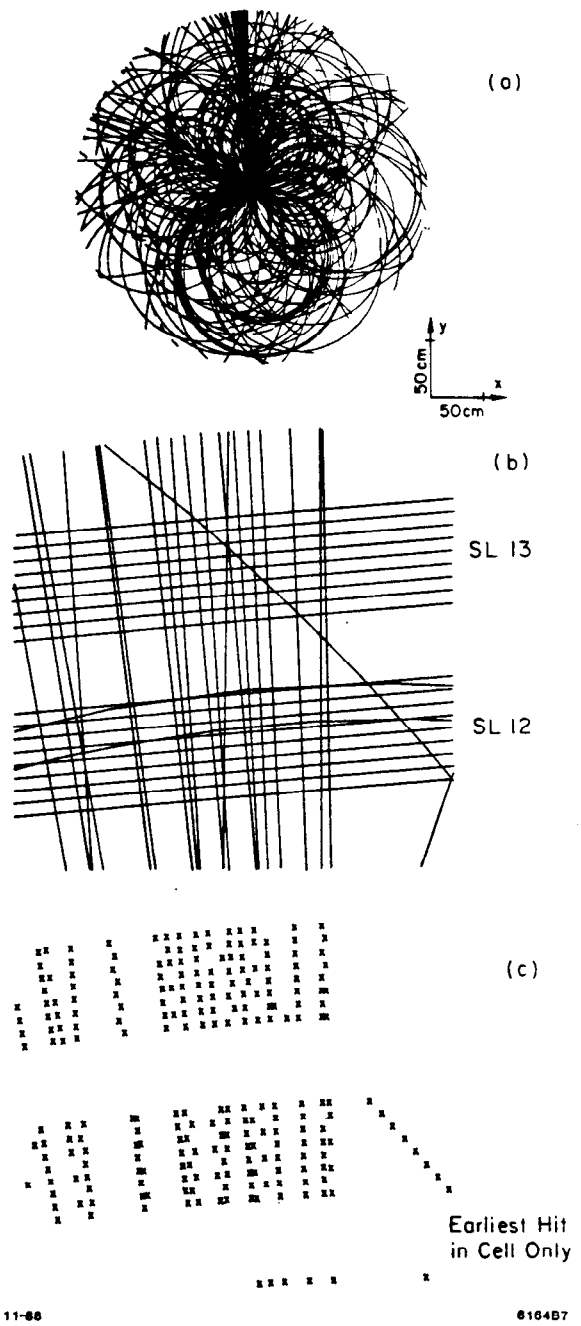

Fig. 9. (a) Two-jet event from ISAJET with $p_T > 1$ TeV/c in a 2-Tesla magnetic field in a detector of the geometry of the Large Solenoid Detector. There are 223 particles with $p_T > 200$ MeV/c and $|\eta| < 1.5$. Converted photons and background from minimum bias events are not shown. (b) Enlargement of the event in the outer two superlayers in the area of the dense jet at the top of the detector. (c) Earliest hit in each cell for the tracks shown in (b).

12,000 – 30,000 digitizations, as shown in Fig. 11(a). The fraction of digitizations from the minimum bias background events is shown in Fig. 11(b). On the average 57% of the digitizations were due to background events. For all tracks (11.6 ± 0.7)% of the digitizations were lost because of the double-hit resolution, and the loss was about the same in all superlayers. For the leptons from the Higgs decay an average of (7.3 ± 0.6)% of the digitizations were lost with the worst losses being in the inner superlayers.

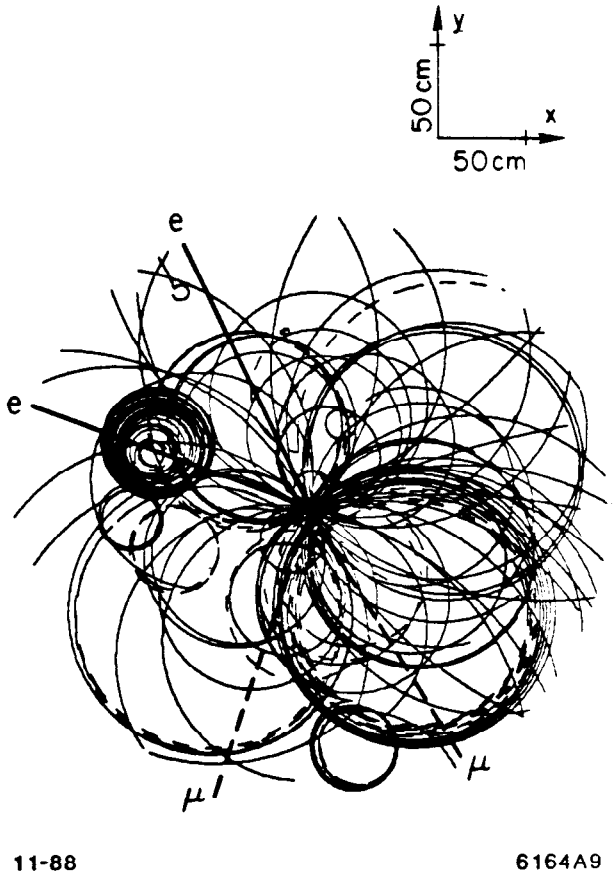

Fig. 10. Example of a Higgs event in the simulated central tracking system. The leptons from the Higgs decay are indicated by the heavier lines. Converted photons and other interactions with the material are included.

3.3. Pattern Recognition

We began working on pattern recognition algorithms in order to examine our original design goals of finding track segments in superlayers and removing hits

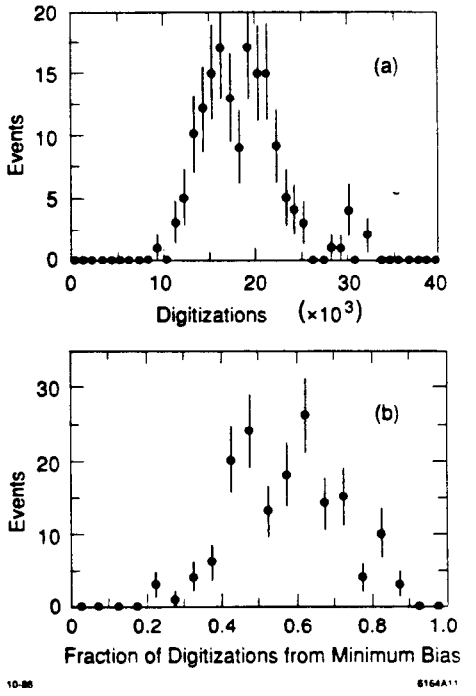

Fig. 11. (a) Total number of digitizations in Higgs events, including digitizations from minimum bias background events. (b) Fraction of digitizations from the minimum bias background events. The mean is 0.572 ± 0.011.

from out-of-time bunch crossings. We also wanted to make the algorithm simple with the hope of using it in the trigger. The algorithm for finding track segments was the following:

1. In each superlayer we identified "roads" containing hits. There are two parameters which can be varied: the width of the road and the number of hits required on the road. We used a width of five wires and required three or more hits out of eight possible. For isolated tracks one could require more hits; however, if two tracks are close together, as in Fig. 9, they will produce hits only on alternate layers and if one is lost due to the double-hit resolution there will be only three hits. The road requirement discriminates against low-p_T tracks.

2. We required that at least one of the hits be in a layer with the opposite wire stagger from the others so that the left-right ambiguities could be resolved and hits from out-of-time bunch crossings rejected.

3. We required that the hits be consistent with a straight line to within an error and in the process resolved the left-right ambiguities. Of course, the tracks approximate straight lines only locally within the superlayer, and the spatial resolution must also be taken into account.

Figure 12(a) shows all of the digitizations[15] for the event shown in Fig. 10, including those from minimum bias background events. Figure 12(b) shows only those digitizations which are included in segments. Keeping only those digitizations which form segments cleans up the events considerably. Figure 12(c) shows the tracks from the original event in the outer five superlayers in the region around the muon at the lower right. Figure 12(d) shows all of the digitizations in the event in the enlarged region (the digitizations are displayed at the locations of the hit wires). Finally, Fig. 12(e) shows only those digitizations which form track segments; here, the left-right ambiguities have been resolved, the drift times have been converted to distances, and the digitizations are displayed at the positions of closest approach of the tracks to the wires. One can clearly identify the muon track, and most of the extra hits have been removed.

Next, we applied our segment-finding algorithm to the e and μ tracks from Higgs boson decays. We defined two classes of segments: a "good" segment was one with at least five hits from a lepton track and no other hits, and an "OK" segment was one with at least five hits from the lepton track and one hit from another track. The effects of hits from other tracks remain to be studied; we plan to compare measured momenta with produced momenta in future work. With these definitions, we counted the number of segments found for each lepton track.

The distribution of the number of good segments for the e's and μ's in the Higgs events is shown in Fig. 13(a). The corresponding distribution of total (good or OK) segments is shown in Fig. 13(b). We see that the lepton tracks from Higgs decay have an average of about 8 good segments and 10 total segments out of 13 possible. Typically 30–50% of segments were good in the inner superlayers, increasing to almost 80% for the outer superlayers. When OK segments are counted as well, 50–60% of segments are accepted for inner superlayers and over 80% for outer superlayers.

3.4. Future Work

We are planning to continue our tracking simulation studies using the software we have developed. Future work will include simulation of small-angle stereo wires and cathode pads or strips for reconstruction of the direction along the wires; linking of segments, both axial and stereo, to form tracks; studying how much additional information is needed from cathode pads or strips to link the stereo segments properly; a more realistic simulation of electron drift in small-cell or straw tube

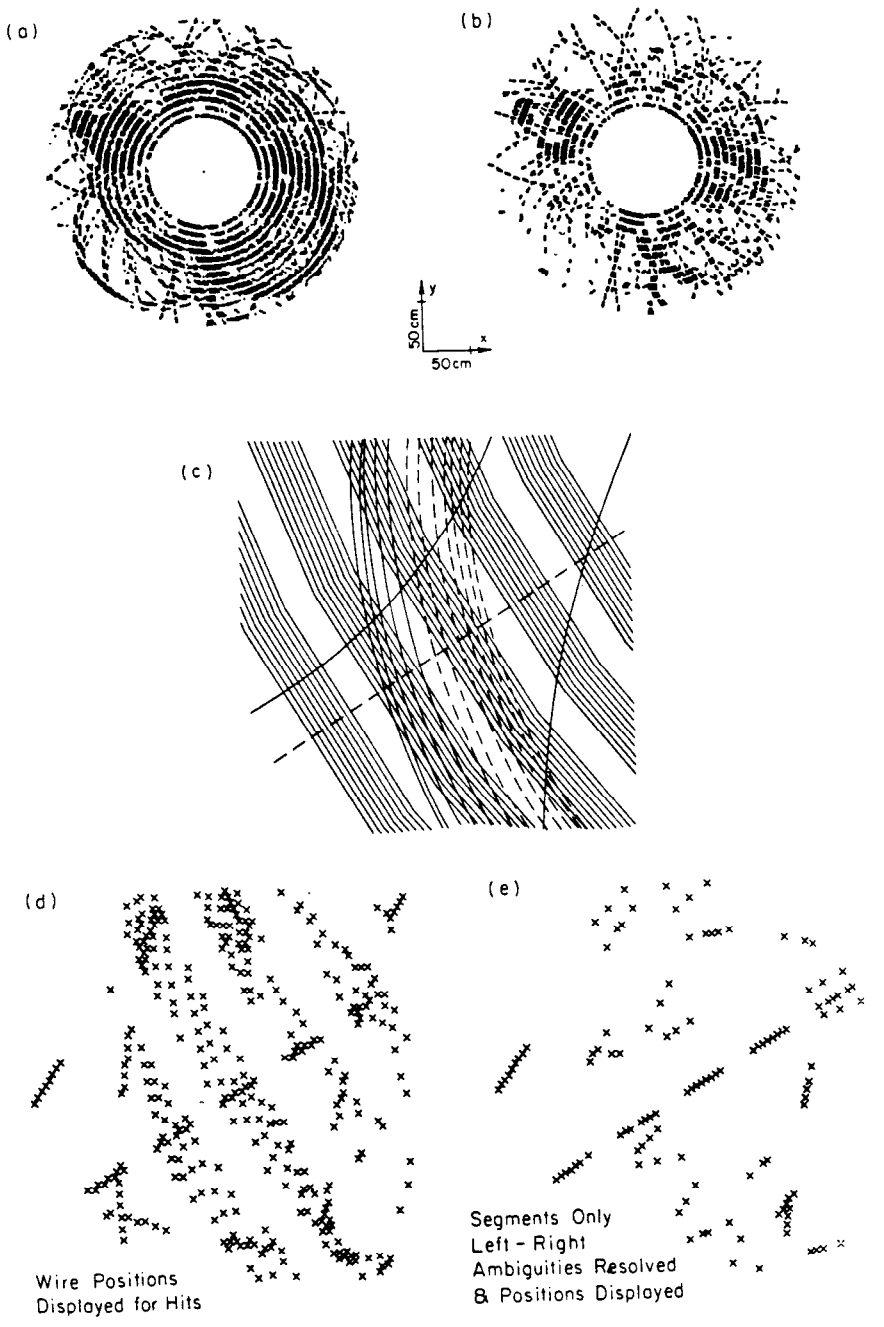

Fig. 12. (a) All of the digitizations for the Higgs event shown in Fig. 10, including those from minimum bias background events. (b) Digitizations for this event which are included in track segments, as defined in the text. (c) Tracks from the original event in an enlarged region in the outer five superlayers in the region around the muon at the lower right. (d) All of the digitizations in the event in the enlarged region of (c) (the digitizations are displayed at the locations of the hit wires). (e) Only those digitizations which form track segments in the enlarged region. Here, the left-right ambiguities have been resolved, the drift times have been converted to distances, and the digitizations are displayed at the positions of closest approach of the tracks to the wires.

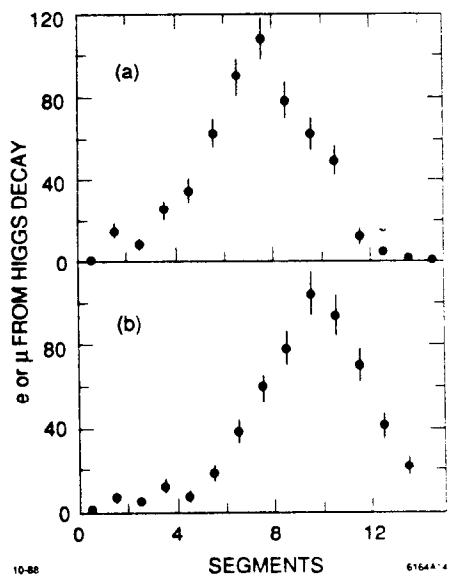

Fig. 13. (a) Distribution of the number of good segments out of 13 possible for the e's and μ's from the Higgs decays. (b) Distribution of the number of total segments (good or OK) for the leptons from the Higgs decay.

drift chambers, including the effects of $\mathbf{E} \times \mathbf{B}$; and conceptual design and simulation of intermediate tracking, as described briefly in Section 2.3.5. In addition, we will study tracking for different physics processes, such as new heavy fermions, supersymmetric particles, and high-p_T two-jet events, and begin to develop a realistic design for a tracking system for a complete SSC detector, including other detector components.

4. IMPLICATIONS FOR TRIGGERING AND DATA ACQUISITION

We have shown that an SSC tracking system design based on a pattern recognition strategy of finding track segments in superlayers appears to provide a powerful means of finding tracks in complex SSC events, even in an environment of multiple events from several bunch crossings. So far, detailed simulations have verified the concepts developed over several years for SSC tracking detectors. An algorithm for finding track segments such as that described here could be used in the trigger for high-p_T tracks. Depending on the effects on the physics analyses, we might envision making this requirement at the processor level, reading out only the hits that form track segments or even just the segments themselves.

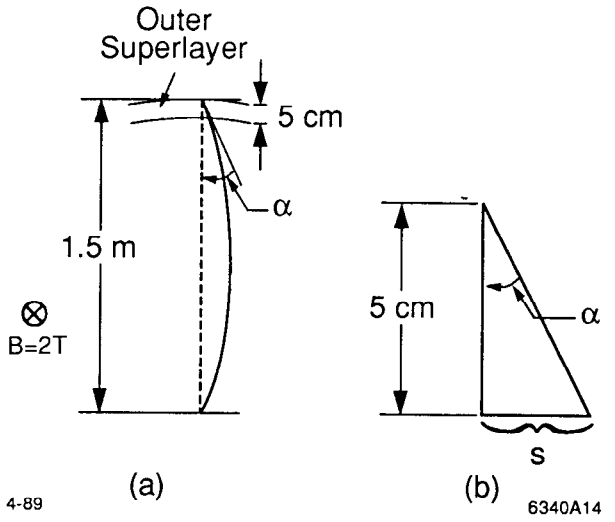

Fig. 14. (a) Illustration of the angle α between a radial line and the tangent to a track at the exit point of the track from the outer superlayer. (b) Illustration of the displacement s of a track from a radial line across the depth of a superlayer.

Track segments in superlayers can be characterized as local straight line segments since the sagitta over a superlayer is too small to measure for a relatively high p_T track. The two parameters characterizing a line segment could be the slope relative to a radial line at the track segment and the position given by the azimuthal angle. The slope is a measurement of the p_T of the track. The geometry for an outer superlayer is illustrated in Fig. 14. The radial extent of an outer superlayer is about 5 cm at a radius of about 1.5 m. The angle α is the angle between the tangent to the track at the outer superlayer and a radial line at the exit point of the track from the superlayer. The distance s is the displacement of the track from the radial line over the width of the superlayer. Table 3 shows the relationship between the angle α and the displacement s for various p_T values for a solenoidal magnetic field of 2 Tesla.

On the basis of these dimensions, one could imagine requiring $p_T > 50$ GeV/c in the trigger, but drift times are needed in the segment finding. An added complication is the need to have an estimate of the position of the track along the length of the wire since the propagation time is about 16 ns. Once track segments are found, they can be matched to clusters in the calorimeter, for example.

The triggering and data acquisition systems should be designed in such a way

Table 3. Angle Between Track Segment and Radial Line and Displacement Across Outer Superlayer for Tracks at Various p_T Values

p_T (GeV/c)	$\sin\alpha$	s (mm)
10	0.045	2.25
50	0.009	0.45
100	0.005	0.23
500	0.001	0.05

that they can evolve to greater sophistication as more is learned about the detector and background conditions. At first, we would need to read out all of the data and the track segments, presumably at lower than design luminosity, in order to find the constants for the time-distance relations in the straw tubes and the geometric positioning, optimize the tracking code, and check the segment-finding algorithms. Then later we might read out only the hits which make up the track segments along with the track segments. Finally we might gain enough experience to read out only the segments. However, we would always need to have the capability to read out all of the hits for at least some of the events in order to update constants for the time-distance relation and check the segment-finding algorithms.

Although a great deal of work remains to be done, we are optimistic that an SSC tracking system based on finding local track segments, whether in straw tubes or in silicon, will enable us to explore the new physics which awaits us in the SSC regime.

ACKNOWLEDGMENTS

We would like to thank members of the SLD Collaboration at SLAC, especially D. Aston, for their help in getting GEANT running on the SLAC IBM computer and for providing the interface to GEANT graphics. We also thank the organizers of the Workshop, particularly R. Orr, for providing such a stimulating environment. We gratefully acknowledge the support of the Department of Energy Program for Generic Detector Research and Development for the SSC.

REFERENCES

1. D. G. Cassel, G. G. Hanson *et al.*, "Report of the Central Tracking Group," *Proceedings of the 1986 Summer Study on the Physics of the Superconducting Supercollider*, edited by R. Donaldson and J. Marx, Snowmass, CO, 1986, p. 377.

2. *Radiation Levels in the SSC Interaction Regions*, Task Force Report, edited by D. E. Groom, SSC–SR–1033, SSC Central Design Group, June, 1988. For relativistic particles, rapidity and pseudorapidity can be used interchangeably. The pseudorapidity variable is given by $\eta = -ln\ (tan\ \theta/2)$ where θ is the angle relative to the beam direction.

3. *Report of the Task Force on Detector R&D for the Superconducting Super Collider*, SSC-SR-1021, SSC Central Design Group, June, 1986, pp. 44-60; M.G.D. Gilchriese, *Proceedings of the 1984 Summer Study on the Design and Utilization of the Superconducting Super Collider*, edited by R. Donaldson and J. G. Morfin, Snowmass, CO, 1984, p. 607; G. Hanson and D. Meyer, *ibid.*, p. 585.

4. J. Va'vra, *Proceedings of the Workshop on Radiation Damage to Wire Chambers*, edited by J. Kadyk, Lawrence Berkeley Laboratory, Berkeley, CA, 1986, p. 263.

5. A. H. Walenta, Nucl. Instr. and Meth. **217**, 65 (1983).

6. R. Thun, "Prospects for Wire Chambers at High Luminosity," to be published in *Proceedings of the 1988 DPF Summer Study on High Energy Physics in the 1990's*, Snowmass, CO, June 27–July 15, 1988.

7. R. DeSalvo, "A Proposal for an SSC Central Tracking Detector," CLNS 87/52.

8. R. J. Cashmore, S. Ozaki, and G. Trilling, "Summary and Comparison of High p_T Detector Concepts," *Proceedings of the Workshop on Experiments, Detectors, and Experimental Areas for the Supercollider*, edited by R. Donaldson and M.G.D. Gilchriese, Berkeley, CA, 1987, p. 301.

9. R. L. Gluckstern, Nucl. Instr. and Meth. **24**, 381 (1963).

10. G. G. Hanson, S. Mori, L. G. Pondrom, H. H. Williams *et al.*, "Report of the Large Solenoid Detector Group," *Proceedings of the Workshop on Experiments, Detectors, and Experimental Areas for the Supercollider*, edited by R. Donaldson and M.G.D. Gilchriese, Berkeley, CA, 1987, p. 340.

11. I. Hinchliffe and E. M. Wang, "Effect of Lepton Energy Resolution on Higgs Searches at the SSC," to be published in *Proceedings of the 1988 DPF Summer Study on High Energy Physics in the 1990's*, Snowmass, CO, June 27–July 15, 1988; E. M. Wang, G. G. Hanson *et al.*, "Higgs $\rightarrow$ Four Leptons at the SSC," *ibid.*.

12. F. E. Paige and S. D. Protopopescu, "ISAJET 5.30: A Monte Carlo Event Generator for pp and $\bar{p}p$ Interactions," in *Proceedings of the 1986 Summer*

Study on the Physics of the Superconducting Supercollider, edited by R. Donaldson and J. Marx, Snowmass, CO, 1986, p. 320. (The current version of ISAJET is 6.12.)

13. R. Brun, F. Bruyant, and A. C. McPherson, *GEANT3 User's Guide*, CERN DD/EE/84–1.
14. A. P. T. Palounek, "Simulating a Central Drift Chamber for a Large Solenoid Detector at the SSC," SLAC–PUB–4787.
15. The GEANT3 graphics does not display digitizations, only hits. To display digitizations, they must be converted to spatial coordinates and stored in the hit bank.